

Mosaic Energy Landscapes of Liquids and the Control of Protein Conformational Dynamics by Glass-Forming Solvents

Vassiliy Lubchenko* and Peter G. Wolynes

*Department of Chemistry and Biochemistry, University of California at San Diego,
La Jolla, California 92093-0371*

Hans Frauenfelder

Theory Division, T10, Los Alamos National Laboratory, Los Alamos, New Mexico 87545

Received: October 20, 2004; In Final Form: January 24, 2005

Using recent advances in the Random First-Order Transition (RFOT) Theory of glass-forming liquids, we explain how the molecular motions of a glass-forming solvent distort the protein's boundary and slave some of the protein's conformational motions. Both the length and time scales of the solvent imposed constraints are provided by the RFOT theory. Comparison of the protein relaxation rate to that of the solvent provides an explicit lower bound on the size of the conformational space explored by the protein relaxation. Experimental measurements of slaving of myoglobin motions indicate that a major fraction of functionally important motions have significant entropic barriers.

1. Introduction

Proteins are nanoscale machines operating in a solvent environment. Owing to the small size of proteins, no part of any protein is very far from the solvent, so it is no surprise that some important protein rearrangements follow solvent motions over a broad range of times and temperatures, a behavior that we call slaving.¹ At room temperature, most (but perhaps not all) solvent motions are very much faster than most protein conformational changes, so it is natural to average over these motions as in the theory of Brownian motion. In this case we can think of protein motions as Brownian trajectories that are highly damped by solvent friction describing evolution on a free-energy landscape averaged over solvent coordinates. To understand the behavior at physiological temperatures it turns out to be important to understand protein motions under nonphysiological conditions. In an effort to elucidate the protein energy landscape and separate out various biologically important motions, biochemistry has been taken into the cryogenic realm. Ringe and Petsko have emphasized the potential of cryochemical techniques to resolve many enzymological puzzles.² In this cryogenic regime, however, the solvent dynamics slows down tremendously, and it is essential to be able to quantify how protein motions are affected by the solvent in this extreme limit that seems opposite to the limit of Brownian motion theory. Experimentally a great deal is known. Detailed studies show some protein motions whose temperature dependence follows faithfully the solvent, while for other motions, there is a near or even complete independence of the protein dynamics from the reconfiguring solvent. The experimental work has been clouded by the lack of a theory for these motions of the neat liquid. Recently many quantitative features of solvent dynamics, which ultimately lead to the glass transition, have been explained by a theory that shows deeply supercooled liquids have a

complex dynamical mosaic structure.^{3–6} When the solvent is supercooled the protein lives in a frozen sea of amorphous icebergs. The purpose of this paper is to show how our theoretical understanding of this mosaic structure allows us to predict whether a protein motion will be slaved to the solvent's mosaic structure or not. This prediction relies on the comparison between the distance a protein subunit must move and a length scale characterizing the motional freedom in the liquid mosaic, the so-called Lindemann length.⁷ The latter is the amplitude of a typical thermal lattice vibration at the melting point and reflects typical molecular displacements on the edge of mechanical stability of a crystal or glass alike. By combining these theoretical results with the experimental data we can deduce a great deal about the nature and extent of the protein dynamics. While our analysis here focuses on solvent motions in the glassy regime, we note that “bound waters” move slowly even under physiological conditions, and some of the ideas introduced here may therefore be relevant to understanding protein–solvent coupling *in vivo* when these slow solvent modes are of relevance. Actually, while the theory of the solvent glass transition has been constructed for deeply supercooled liquids, the experimental data given in Section 2 demonstrate that slaving occurs from room temperature down to the solvent glass transition temperature, over about 10 orders of magnitude in rate.

The protein motions that are most prone to slaving in a glassy solvent are subject to primarily *entropic* barriers under normal conditions. This will enable us to formulate the arguments in a geometric form, that involves (independently measurable) length scales only, thus rendering the arguments quite general. Further, the conclusions can be cast in a form that is largely independent of the morphology of the conformational space but reflects the *size* of conformational subspaces. A subspace is a subset of states—or a “basin”, in the landscape language,—accessible on a particular time scale and relevant for relaxations within the basin. It is also measurable, in principle, by calorimetry at

* Corresponding author e-mail: vas@mit.edu. Current address: Department of Chemistry, Massachusetts Institute of Technology, Cambridge, MA 02139.

frequencies comparable to the rate of that relaxation. (Alternatively, the subset is sampled by a simulation on the corresponding time scales.) On the other hand, the degree of slowing down of a slaved process, relative to the solvent relaxation, will be shown to directly reflect the size of the conformational subspace explored by a given protein relaxation. We thus explicitly establish the intrinsic relation between *thermodynamic* and *kinetic* characteristics of the protein dynamics. One may draw a revealing analogy with supercooled liquids, where a connection between the kinetic, viscosity anomaly, and the entropy crisis exists.³ In a notable distinction, here we only consider protein relaxations of biological relevance, which require a specific reaction path, something that is statistically irrelevant in neat liquids, whose landscape is rather featureless. The slowing down of a slaved process is, in fact, the price one pays for the specificity. Another, surprising consequence of the specificity is, the more a protein motion is slowed, the more exponential, relative to the solvent, it will appear. (This is actually an example of motional narrowing.) Just as in supercooled liquids, a larger configurational/conformational entropy corresponds to more exponentiality.

The organization of the paper is as follows. We first review the main results on the slaving of protein motions in glass-forming solvents. We then sketch the main ideas of the theory of glassy liquids and their mosaic structure and use these ideas to characterize the main features of the coupling of the protein motions to the solvent.

2. Slaving – The Experimental Background

As pointed out in the Introduction, proteins are not isolated systems as shown in textbooks; they are embedded in a solvent and interact with other biomolecules. These interactions can influence protein motions and protein functions. Experiments involving a broad range of proteins demonstrate that protein motions can be categorized into (at least) three different classes:

Slaved Motions.¹ The rate coefficient $k_s(T)$ of slaved motions approximately follows the dielectric fluctuations in the bulk solvent surrounding the protein, given by $k_\alpha(T)$,⁸ over many orders of magnitude in rate coefficient, but is smaller by a factor $n(T)$

$$k_s(T) = k_\alpha(T)/n(T) \quad (1)$$

$n(T)$ can be as large as 10^5 .

Hydration-Shell Coupled Motions.⁹ These motions follow the dielectric relaxation in the hydration shell of the proteins but are also slower. Over a broad temperature range, they are faster than the slaved motions. They appear to be largely independent of the motions in the bulk solvent and exist even if the bulk solvent is rigid.

Nonslaved motions are essentially independent of the surrounding but can be influenced by vibrations.

In the present paper, we do not take account of the inhomogeneous behavior caused by the water layer but consider only the first and last classes, motions slaved to the bulk solvent or completely unslaved. A large number of experiments yield information about dynamic processes in proteins. We use representative data from a small set of such experiments, flash photolysis,^{10–12} pressure release,^{13,14} and spectral hole burning.¹⁵ Some examples of slaved processes are given in Figure 1, where data taken from experiments with myoglobin (Mb) are shown. Mb can assume three major structures or taxonomic substates, denoted by A_0 , A_1 , and A_3 .^{12,17} In A_0 , dominant at low pH, Mb catalyzes reactions among small molecules. In A_1 , Mb stores

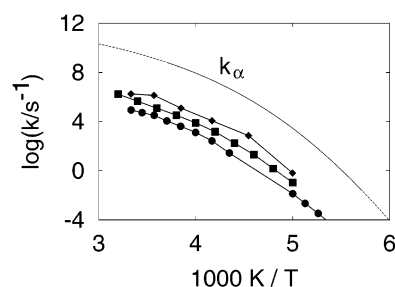


Figure 1. The temperature dependence of the rate coefficients for fluctuations in the solvent (k_α , ref 16), for the exchange between the taxonomic substates A_0 and A_1 (●), for the exit of CO molecules from the protein (■), and for fluctuations after hole burning (◆). The solvent is 3/1 v/v glycerol/water.

dioxygen. The function of A_3 , if any, is not known. The structures of A_0 and A_1 have been determined:¹⁸ In A_0 , the distal histidine extends into the solvent; in A_1 , it is in the heme pocket. The rate coefficients in Figure 1 refer to the following processes in Mb: k_α ($= k_{\text{diel}}$) characterizes the dielectric fluctuations in the solvent, 3/1 v/v glycerol/water. k_{exit} gives the exit of a CO molecule after flash photolysis from the protein, k_{01} is the exchange rate between the substates A_0 and A_1 , and k_{fluct} is the fluctuations after hole burning.

The concept of slaving emerges from Figure 1. The processes shown have essentially the same temperature dependence as the bulk solvent but are slower than k_α by the factor $n(T)$ in eq 1. $n(T)$ is approximately temperature independent and ranges from near 1 to about 10^5 . The data raise a number of questions: What is the mechanism of slaving? Why are the slaved processes slower than k_α ? Is more information than just $n(T)$ hidden in the data?

A descriptive answer to the second question has been given earlier:¹ The exit of a CO from Mb is not a one-step process. It involves a large number of small structural changes in the protein, each approximately given by k_α . The slaved processes can thus be described as a Brownian walk in conformation space from an initial substate to the substates with an open exit. In the present paper we give a quantitative explanation of slaving, based on the Random First-Order Transition Theory (RFOT).

The primary property of slaving following from the experimental data and expressed by eq 1 is not the only information that can be extracted from the experiments that have already been performed. Processes in complex systems such as proteins are usually nonexponential in time; their rate coefficients are not single valued but must be described by a distribution. The RFOT theory and the picture of a random walk in conformation space suggest that the distribution should narrow as the system makes more steps or, in other words, that slaved processes with large $n(T)$ could even be exponential in time. Preliminary evidence for such a behavior exists,^{13,14} but more experiments are needed to explore this aspect.

3. Dynamics of Supercooled Liquids: Overview of the Random First-Order Transition Theory and its Microscopic Implications

Processes within a completely folded protein interact with the solvent motions through the protein/solvent boundary. In a partially *unfolded* protein, small fragments of the peptide chain may be directly exposed to the solvent. In either case, the effects of the solvent on a protein can be systematically described with the knowledge of the length scales of the solvent motions and the time scales on which these motions occur.

In contrast to ordinary liquids above the melting point, molecular transport and relaxation in deeply supercooled liquids are activated, slow and involve cooperative rearrangements of many molecules. These cooperative motions occur on a distributed range of relaxation times and are characterized by a number of length scales. On the other hand, a number of *thermodynamic anomalies also* distinguish supercooled liquids from their truly equilibrium counterparts. The kinetic and thermodynamic peculiarities of supercooled fluids are intrinsically related and cannot be understood one without the other. In this Section, we briefly outline the phenomenology of glass forming melts, and review the microscopic picture of these phenomena based on the Random First-Order Transition (RFOT) theory of the glass transition.^{3,4} This microscopic picture will be subsequently used to rationalize and quantitatively understand slaving of internal protein fluctuations to the solvent.

Imagine a liquid being cooled below its boiling point. Assume, for the sake of argument, that the material has only one crystal structure. Once the liquid is cooled somewhat *below* the melting temperature T_m , at which the bulk free energies of the liquid and crystal states are equal, growing a crystal nucleus becomes subject to a *finite* barrier. If cooled sufficiently slowly, the liquid will thus crystallize. Conversely, by realizing a fast enough cooling schedule, it is possible to overcool the fluid substantially below T_m without crystallizing. Under these circumstances, the rate of molecular relaxations, it turns out, rapidly decreases with temperature, approximately obeying the empirical Vogel–Tamman–Fulcher (VTF) law

$$k_{\text{VTF}} = k_{\text{micro}} e^{-D T_0 / (T - T_0)} \quad (2)$$

where k_B is the Boltzmann constant and T_0 is the temperature where k_{VTF} would vanish. D is called fragility. The prefactor k_{micro} is of the order a 10^{12} sec^{-1} . It corresponds, as we will see shortly, to molecular scale nonactivated events, roughly of the order a few vibrational time scales. Moving the liquid/crystal interface, when growing a crystal nucleus, is subject to viscosity. The latter decreases dramatically with temperature, according to the general dependence in eq 2. The true equilibrium, crystal state thus becomes virtually kinetically inaccessible, actually helping maintain the system in the fluid state. On the other hand, relaxation rates characterize local equilibration rates, of course. As a result, processes with rates $k > k_{\text{VTF}}$ encounter an essentially elastic response from the medium, the same way a sample of molasses recovers its shape after a quick perturbation. In contrast, if subjected to a steady force, molasses will exhibit a liquid response, i.e., it will flow. Since structurally the system is a liquid, one may conditionally designate this liquid response as “equilibrium”, bearing in mind that the crystal state is, again, behind an effectively unsurmountable free energy barrier, while all thermally relevant *liquid* states are kinetically accessible. Suppose further one cools the fluid so fast that equilibrating to the new temperature requires local relaxation rates to exceed the relaxation rate from eq 2. As a result, the liquid can no longer exhibit this conditionally “equilibrium” response at *any* frequency no matter how low. Alternatively, the system response no longer shows time-translational invariance on any time scales no matter how long. (The so-called “aging” thus takes place, characterized, for example, by a dependence of the system response on the sample’s history prior to measurement.) This kinetic singularity, called the glass transition, is also accompanied by a rather sharp jump in the heat capacity, detected by differential calorimetry. One can define the glass transition temperature T_g , in a precise way, as the lowest temperature at which the liquid exhibits fully equilibrium response (in the

conditional sense explained above) in a frequency range of nonzero measure, given a particular quenching schedule. The most probable liquid relaxation rate, i.e., k_{VTF} itself, at the glass transition will reflect the characteristic time scale of the quench, as already mentioned. (The precise relation depends on the specific cooling schedule.) For routine laboratory quenching rates, $k_{\text{VTF}}(T_g)$ varies within 10^{-2} – 10^{-4} s^{-1} . On the faster side, quenching rates are limited by the substance’s thermal conductivity, of course, while achieving progressively slower rates is only a matter of the experimenter’s patience and ability to maintain stable temperature conditions.

Integrating the heat capacity in temperature gives one the amount of the liquid entropy in excess of the corresponding crystal (assuming the *vibrational* entropies of the two states are similar). This excess entropy corresponds to all the *translational* degrees of freedom in the system that ordinarily would freeze out at the moment of crystallization and give rise to a latent heat. Instead, when crystallization is avoided, these degrees of freedom freeze out gradually, as signified by a rapid but still continuous temperature dependence of the local equilibration time scale in eq 2. Now, the excess entropy is usually called “configurational entropy”, which we will denote as s_c . As just mentioned, s_c gradually decreases with lowering the temperature but stays put below T_g because the structure no longer equilibrates but remains almost the same as of the moment of vitrification, subject only to minor changes due to aging.¹⁹ The resulting slope change in the temperature dependence of s_c , at T_g , corresponds to the heat capacity jump at the glass transition, of course. If, nevertheless, one extrapolates s_c *below* T_g , as though to emulate “equilibrium” cooling, one discovers that the configurational entropy would *vanish* at some positive temperature T_K . This entropy crisis was first emphasized by Kauzmann.²⁰ Empirically, the temperatures T_K and T_0 are always near each other, see e.g. ref 21.

That this is no coincidence can be rationalized by the following, qualitative argument: Below the melting point, the liquid is empirically known to be dense, almost as dense as the corresponding crystal; it is also metastable globally and, a fortiori, locally. In order for a given molecule to perform a translation, as opposed to vibrating within its current metastable potential cage, a number of surrounding molecules, too, must rearrange so as to conform to the new location of that given molecule. As temperature is lowered, the lattice becomes denser; there are fewer ways to aperiodically pack the molecules subject to this higher density constraint. As a result, a larger number of surrounding molecules would need to move in order to conform to a new location of a given moving molecule. Molecular commotions of such a larger spatial extent are less likely, implying higher barriers. Therefore, having fewer structural states, and hence a smaller configurational entropy, leads to slower, increasingly cooperative molecular transport.

The RFOT theory formalizes these qualitative notions and builds a microscopic picture of transport and thermodynamics in supercooled liquids step by step. First, the emergence of the metastability can be understood as a dynamical transition, at a temperature T_A , in which molecules give up their ideal gaslike translational entropy in favor of forming metastable structures, or “cages”, that live for several hundred vibrational periods. Transport changes qualitatively as a result: In place of collisionally interrupted “flights”, each molecule undergoes small displacements at a time by destroying its current cage and subsequently forming a new one, characterized by a distinct molecular arrangement. Each such displacement is the typical vibrational amplitude in a solid at melting, i.e., on the edge of

mechanical stability. The corresponding length scale, d_L , was first introduced by Lindemann⁷ and is empirically known to be around 1/10 of the molecular spacing for all substances. In supercooled liquids, it is seen directly in neutron scattering.²² There, a plateau in the structure function $S(k, t)$ shows that particles are “caged” to remain within d_L of their local minimum energy configuration for long periods of time before escaping. The transition (more precisely a smooth crossover) at T_A was discovered in liquid density functional studies^{23,24} and Mode Coupling Theories,^{25,26} as the appearance of a metastable minimum on the free energy surface, much like during a spinodal transition, except the number of distinct phases is large. A distinct length scale emerges, during the transition, that gives the location of the metastable minimum. (The transition itself is therefore first order.) This length is the Lindemann length d_L itself.

The RFOT theory proceeds further to formally describe the cooperative transport events, discussed earlier, that occur by activated transitions between distinct local aperiodic packings.^{4–6} These transitions are actually “mini-nucleation” events of one aperiodic structure within another. They play the role of the random first-order transition analogues to critical nucleation clusters in ordinary crystalline freezing processes. By virtue of being at equilibrium for times longer than the kinetic energy equilibration time, each of the metastable molecular configurations must locally minimize the liquid free energy functional. There are $e^{s_c N/k_B}$ of the free energy minima for each region containing N molecules, where s_c is the configurational entropy per particle. Motions between these minima are the configurational degrees of freedom in the supercooled liquid. A specific instantaneous molecular arrangement corresponds to a particular mosaic pattern of the metastable clusters. What is the free energy of reconfiguring this mosaic? If it were to cost no energy for a region of size N to explore all of the available $e^{s_c N/k_B}$ distinct configurational substates, the free energy would be $-T s_c N$. However, one state can replace another only by first creating its nucleus inside that old state and then growing the droplet. Thus the issue of the interface energy between different states is important. A detailed argument, using a density functional theory, tells us that the surface tension coefficient for a droplet of a molecular size a is equal to⁴

$$\sigma_0 = \frac{3}{4} \frac{k_B T}{a^2} \ln \left(\frac{a^2}{d_L^2 \pi e} \right) \quad (3)$$

We will elaborate more on the molecular scale “ a ” later, but for now say that it is the size of an independently moving molecular unit. The result in eq 3 is the result of a detailed calculation. Still, its basic scaling with the parameters of the theory can be understood using the following simple notion. Recall the formula for the free energy of a monatomic gas per particle

$$-f = \frac{3}{2} k_B T \ln \left[\left(\frac{eV}{N} \right)^{2/3} \frac{mT}{2\pi\hbar^2} \right] \quad (4)$$

Surface tension is the free energy cost of having a highly strained region between two distinct, nonmatching local packings. These highly strained regions emerge upon supercooling the fluid and contribute to the free energy surplus relative to the lowest energy, crystalline state. Further, the highest stress sustainable by the lattice is that produced by an atomic displacement of the Lindemann length d_L , as already mentioned. Consistent with this, the surface energy due to σ_0 is one-half of

the free energy cost of the free energy loss of a particle forced to be within a (localization) length d_L instead of the allowed length a , corresponding to the liquid’s volume per molecule $V/N = a^3$ and relevant to interchanging the identities of the particles. Recall that $d_L/a \approx 1/10$ for all substances thus rendering the aperiodic structure/structure interface tension a universal quantity, depending only on the energy scale given by the temperature itself. Knowing d_L/a thus allows us to determine the magnitude of the surface tension and consequently formulate the free-energy profile $F(r)$ of the solution-within-solution droplet growth as a nucleation theory

$$F(r) = 4\pi\sigma(r)r^2 - \frac{4\pi}{3}r^3 T \tilde{s}_c \quad (5)$$

where \tilde{s}_c is now the configurational entropy per unit volume, which, recall, vanishes at T_K according to $s_c \approx \Delta c_p (T - T_K)/T_K$. Here, Δc_p is the measurable heat capacity jump at the glass transition. An important aspect of the RFOT theory is that the apparent surface tension coefficient turns out to be radius dependent: $\sigma(r) = \sigma_0(a/r)^{1/2}$,⁴ where σ_0 is the molecular surface tension discussed earlier. The precise form of the interface energy scaling, $r^{3/2}$, differs from the usual r^2 scaling that would apply to a thin two-dimensional interface. The sharp interface between two arbitrary aperiodic free energy functional solutions can almost always be “wetted” by yet other, better matching, solutions.²⁷ There is an exponentially large number of such solutions, as we have noted earlier. Interpolating those intermediate phases (“wetting the interface”) results in an effective reduction of the surface tension. The term “wetting” is in analogy to the wetting of a solid surface by a condensing film of liquid, which has the effect of lowering the surface energy of the gas–solid interface. This reduction is larger for a flatter interface. Such wetting does not generally occur for the solid–liquid interface in a regular crystallization transition, because the crystalline molecular arrangement is equally structurally different from any liquid packing and therefore results in a large mismatch energy upon contact between those two phases. [Occasionally, in forming periodic crystals, an interpolating metastable phase does occur, much like in Ostwald’s rule, well-known in metallurgy.^{28,29}] On the other hand, for aperiodic structures, there exists a near structural continuum within the set of those structures. This continuum of possibilities leads to softening of an otherwise sharp and thus costly interface.

Using this nucleation argument, we are now ready to visualize how a supercooled liquid flows at the molecular level. Owing to the dense character of molecular packing, a translation of a single molecule is accompanied by rearranging the surrounding molecules within a certain cooperative length. The size of this length is determined by the equilibrium size ξ corresponding to the equality of the initial and final free energies of the nucleation profile from eq 5,⁴ $F(R) = 0$. We find $R = 3a(\sigma_0/T\tilde{s}_c a)^{2/3}$. For consistency with earlier papers, we define ξ as the size of a cube with the same number of molecules as within the cooperative radius: $\xi = (4\pi/3)^{1/3} R$. The condition $F(R) = 0$ means all the aperiodic structures, relevant at this temperature, are mutually accessible; therefore a region of size ξ is always capable of rearranging³⁰ and hence the notion of cooperativity. Furthermore, each of those molecular translations is generically of length d_L signifying structural distinction between alternative solutions. The length scale d_L and the time scale $1/k_{VT}$ from eq 2 are the important quantities determining the degree of spatial and temporal confinement of a protein due to the slow motions of its solvent surroundings.

The RFOT Theory is essentially a theory of freezing into aperiodic crystals.³¹ Since there are exponentially many aperiodic structures locally, one must be chosen at *random*. The transition into a given such structure, however, has many characteristics of ordinary freezing: it is first order in the sense that the local order parameter, the mean square displacement of particles sustainable while the system remains trapped in a local aperiodically frozen structure, has a discontinuity. While the local order parameter is discontinuous, the multiplicity of random aperiodic structures depends continuously on the temperature. This ensures that no latent heat is released when a liquid becomes trapped in a glassy configuration. Instead, there is a discontinuity in the heat capacity reflecting the gradual freezing out of configurational degrees of freedom. Thus a random first-order transition is thermodynamically a second-order transition, in the Ehrenfest classification.³²

The basic notions of RFOT are quite simple, but they are rich in implications. We finish the discussion of the RFOT theory by listing some of its successful predictions that give us confidence in the correctness of this microscopic picture. At the same time, we will supply additional relevant details for our later discussions. First, one can calculate the barrier from the free energy profile $F(r)$ from eq 5: The critical radius satisfies $\partial F/\partial r = 0|_{r=R^*}$ giving $R^* = a(3\sigma_0/2Ts_c a)^{2/3}$ and $F^* \equiv F(R^*) = 3\pi\sigma_0^2 a/Ts_c$. The latter result immediately yields the Vogel–Fulcher temperature dependence of the relaxation rate, eq 2, because the barrier F^* scales inverse to s_c and s_c scales like $\Delta c_p(T - T_K)$. This formally establishes the otherwise mysterious connection between T_0 and T_K . Not only is the dynamical limit temperature shown to coincide with the thermodynamic entropy crisis, but the theory also predicts the relation between liquid's fragility, i.e., the coefficient in the Vogel–Fulcher law, and the experimentally measurable heat capacity jump

$$D = 32k_B/\Delta c_p \quad (6)$$

where Δc_p is taken per movable unit corresponding to the molecular length scale a from the earlier discussion. Determining the size of the independent moving unit (“bead”) must be done on a particular chemical basis⁴ and is especially straightforward in the case of simple liquids and their mixtures. Here one finds the predicted reciprocal relation between D and Δc_p works particularly well and with the right coefficient. For polymeric solvents, on the other hand, a single bead is most likely to be one or two monomeric units but not the whole chain. In any event, any ambiguity in the bead counting procedure, as far as the value of a and of $d_L \sim 0.1a$ is concerned, is greatly reduced because a is the cubic root of the bead's volume; therefore, any possible resultant error in d_L is always within a few percent. (For a detailed discussion of bead assignment see ref 33.) The RFOT ideas have also explained how the observed degree of nonexponentiality of relaxation rates correlates with the material's fragility (Δc_p or D). The nonexponentiality can be understood as a distribution of relaxation rates around the most probable value, given by eq 2. The distribution, which is roughly log-normal, reflects the fluctuation in energy of the trapped region. Since the energy fluctuations depend on Δc_p , this analysis shows the width of the distribution relative to the most probable barrier is determined by the fragility D according to⁵

$$\delta \ln k_\alpha / \langle \ln k_\alpha \rangle \approx 1/(2 \sqrt{D}) \quad (7)$$

The larger than typical domains are likely to break up into smaller domains, thus “squeezing” the longer time wing of the

distribution into a somewhat narrower band at the most probable k_α .⁵ Again, the resulting distribution agrees well with experiment for a broad range of substances. Note, the Vogel–Fulcher rate k_{VF} from eq 2 corresponds to the most probable rate $k_{\alpha,mp}$ from the relaxation rate distribution $P(k_\alpha)$ and is usually determined as the maximum position of a frequency dependent response function of a liquid (see below).

The cooperative length ξ , alternatively understood as the mosaic length scale, depends only very weakly (logarithmically) on the Lindemann ratio. At the glass transition temperature, it is about 5–6 molecular lengths for *all* substances. Ultimately, this explains the widely universal aspects of supercooled liquid dynamics. Above the glass transition, the temperature dependence of ξ obeys the simple law⁴

$$\xi(T) = \xi(T_g) \left(\frac{T_g - T_K}{T - T_K} \right)^{2/3} \quad (8)$$

near T_K but shrinks faster than this asymptotic behavior as T_A is approached.^{4,33} One should bear in mind that at high enough temperatures, ξ becomes comparable to the molecular scale itself; the picture of cooperative rearrangements obviously must break down at such high temperatures, and other mechanisms of molecular transport and viscosity will become more important. The transition, or rather the smooth crossover signifying this breakdown, occurs near some temperature T_{cr} . The latter is formally defined as the temperature at which the critical radius R^* for cooperative transitions is equal to the molecular scale a itself.³³ Above T_{cr} , the viscosity of the liquids is primarily due to crowding or “jamming” that results from the molecules being too slow to give way to other, equally slow, molecules and thus effectively forming transient cages. These transient cages still are of size of the Lindemann length which slowly merges with the gas collisional mean free path as the liquid density decreases. This jamming effect is the dominant source of viscosity in hard sphere systems at high enough densities and is usually described by mode coupling theories.^{34,25,23} The temperature T_A apparently corresponds, in the mean field limit, also to the temperature at which a liquid would jam completely.³⁵ In real liquids, such a jamming transition would be greatly lowered in temperature owing to the finite dimensionality. Ultimately, jamming is actually avoided because the molecules find a way to move about by distorting bonds, i.e. in an activated fashion, with the activation profile given by eq 5. T_{cr} is the temperature below which the activated transport takes over; it empirically corresponds to viscosities of the order 10 poise.³³ (For comparison, the viscosity of a liquid near its boiling point is about a centipoise; near the glass transition on a 100 s scale, the viscosity is about 10^{12} poise.) Depending on the substance, the T_{cr}/T_g ratio appears to vary between 1.25 for fragile substances and to over 2 for stronger materials.³³ (“Strong” and “fragile” usually refer, respectively, to smaller and larger deviations of $k_s(T)$ from a simple Arrhenius dependence. The former and the latter imply relatively large and small D values, respectively.)

The length scale for cooperativity of molecular motions from eq 8 has been directly measured in nonlinear NMR spin relaxation experiments³⁶ and conforms to the RFOT predictions. The length scale has been independently confirmed by the universal density of excitations in low T glasses, which correspond to tunneling of the mosaic cells frozen in at T_g , regions of size ξ .^{30,37} The finiteness of the cooperativity length has also observable consequences for the microscopic hydrodynamics,³⁸ namely it gives a deviation from Stokes–Einstein continuum behavior. The deviations from Stokes–Einstein are

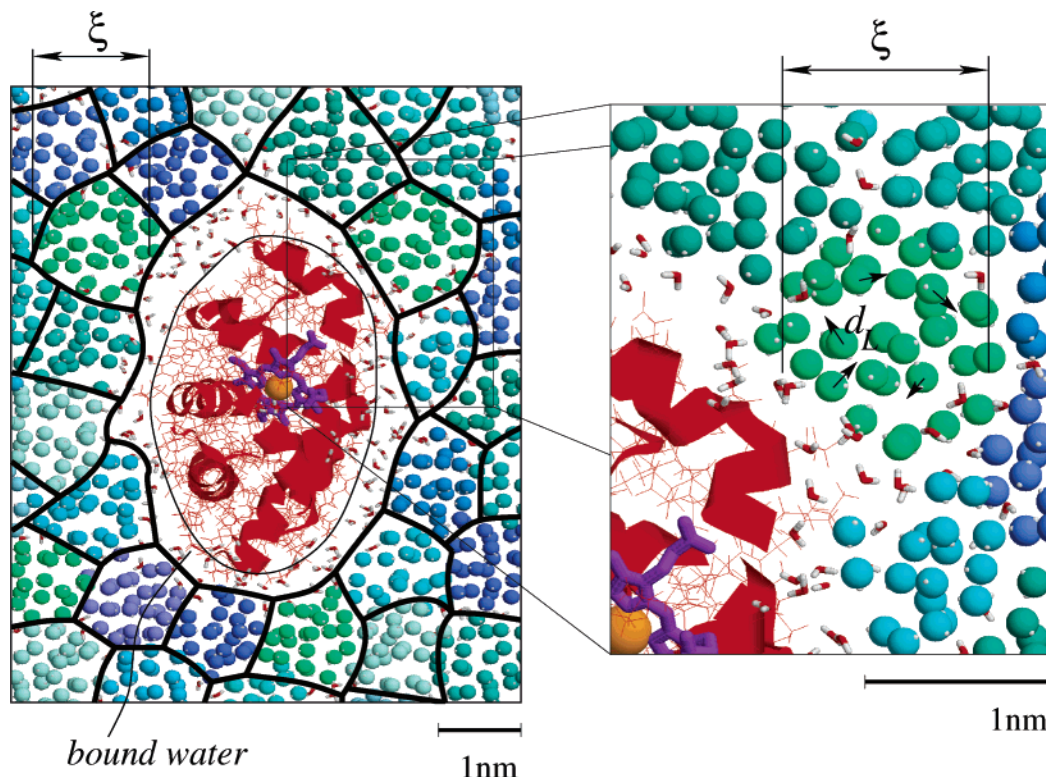


Figure 2. Schematic of a protein imbedded in a vitrified solvent (myoglobin's structure was used). We assume here that only waters are present in the immediate solvation shell. The thick lines denote boundaries between cooperatively rearranging regions, which are also signified by different colors of the solvent molecules. The pane on the right shows a magnified view of a portion of the protein–solvent interface. The small arrows illustrate the molecular translations during a structural rearrangement, that will exert stress on the protein's boundary. Note, the “molecular length scale” a corresponds to the spacing between the solvent molecules. We thank Johan Ulander for his help with the figure.

quantitatively predicted by the RFOT theory.⁶ For internal processes in proteins, the magnitude of ξ is only of marginal importance, but some of its effects may be observed, as we will discuss later.

We finish this section by reiterating those conclusions of the RFOT theory that are particularly relevant for slaving experiments. Immersing a protein in a glass-forming liquid imposes constraints on the protein's shape changes and therefore on any internal processes that cause or depend on such shape changes. The constraints are such that the outer boundary of the protein can only have displacements of size d_L on the time scale distributed around $1/k_\alpha$. These times can be determined independently by means of relaxation measurements on the solvent. The length scale d_L is roughly one-tenth of the size a of an independently moving molecular unit. Large protein motions require many rearrangements of the surrounding solvent regions and take multiples of the time $1/k_\alpha$ to occur. The molecular size a can be varied using different solvents, which offers some freedom in the degree of spatial confinement imposed on the solvated protein. We have thus summarized the molecular mechanism of slaving of the internal processes in proteins to the solvent and the degree of control that can be achieved by slaving. We now turn to an explicit demonstration of some of those conclusions using selected experimental data. A schematic of a protein immersed in a supercooled solvent just above its glass transition temperature is shown in Figure 2. At higher temperatures, the cooperative region size would be smaller, with the T dependence given approximately by eq 8.

4. Slaving of Relaxation in Proteins to the Solvent's Motions

Before we consider possible scenarios of slaving, we must consider how the length scales of the solvent's motions *outside*

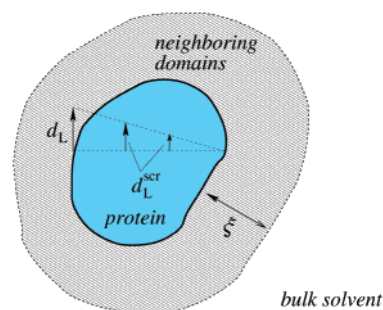


Figure 3. The protein (schematically depicted by the blue blob) is surrounded by a supercooled solvent whose molecules move distance d_L at a time and induce relative distortions d_L^{scr} within the protein. Those solvent motions occur in a cooperative fashion with the corresponding cooperative length ξ being comparable to but normally smaller than the protein's size. If latter is significantly larger than ξ , the “screened” Lindemann length d_L^{scr} is determined by the elastic response of the protein and will depend on the distance r from the protein's surface according to $d_L^{\text{scr}} \sim d_L(\xi/r)^3$, as follows from elementary elasticity theory.

of the protein translate into mutual molecular displacements *within* the protein. There are two distinct possibilities here, both of which lead to very similar conclusions. One possibility is that the protein has many fewer structural degrees of freedom than the surrounding liquid. In this case, the protein can be well modeled as a purely harmonic elastic object and the (screened) molecular displacement *within* the molecule, call it d_L^{scr} , resulting from a perturbing shift of size d_L *outside* can be estimated according to a schematic shown in Figure 3.

As seen, d_L^{scr} is probably scaled down from the original d_L , but the scale is still of the order unity. In the other extreme, the protein could be modeled as part of the liquid itself (this is quite

credible—we know that within the native state basin, the number of conformational states of the protein is still large, see below). In this case, the internal displacement could be somewhat larger than d_L , since the relevant internal molecular length, such as a (possibly hydrated) residue's size, is often larger than the solvent size a . Either way, $d_L^{\text{scr}} \sim d_L$ is probably maintained as a good approximation in most cases; still, we will keep the two parameters distinct for clarity in argumentation.

The other important length within RFOT—the cooperative length ξ , as we have mentioned already, is at most 5–6 molecular lengths at T_g and is smaller much above T_g . It is therefore generally somewhat smaller than the protein's size, except for the smallest proteins or peptides. The relation of the two lengths, ξ and the protein's size, affects the way averaging of the slaved rates with respect to the solvent's relaxation rates k_α is performed. It is, however, easier for us to discuss this issue in the following subsection after we choose a specific description for the internal relaxations.

Now that we understand the mechanism by which the protein's motional freedom is constrained by a slow, supercooled solvent, we can discuss different scenarios of slaving. Owing to the completely classical character of the relaxation, a general analysis at the level of a simple kinetic theory is possible. Depending on within which kinetic class a particular relaxation process falls, a description with more microscopic detail can be developed, which we comment on later in the paper. But first, what are the *a priori* kinetic schemes that can be realized in a protein constrained by a supercooled liquid?

4.1. Case 1: No Intrinsic Barriers. By no intrinsic barrier we mean the situation that applies to processes involving large-scale conformational changes and which, above T_A , would be only subject to the viscous resistive force from the liquid. Examples of such are motions of weakly connected subdomains of a protein or large length scale chain dynamics, where the barrier vanishes by virtue of Kuhn's theorem.³⁹ Upon cooling the solvent below T_A , a barrier will appear because energy is required to rearrange solvent configuration. Examples of such slaved processes in ref 1 include exit of the CO into the solvent and the structural fluctuations allowing transitions between the taxonomic states A_0 , A_1 , and A_3 . The processes may actually involve a partial protein unfolding.⁴⁰ Absence (or a relatively low height) of an intrinsic barrier for these processes is experimentally indicated by the near temperature independence of the ratio of the internal relaxation rate to that of the solvent: (k_s/k_α) . Some care is needed in making this statement since relaxation in a supercooled liquid is characterized by a distribution of times, not just a single time scale k_α^{-1} (especially markedly so for the fragile liquids⁵). Nevertheless, we will show that the presence of a nonzero width of the distribution of reconfiguration times does not lead to any additional T -dependence of (k_s/k_α) , where k_α is determined as the frequency at the maximum of the imaginary part of a measured response function of the liquid. Note also that entropic elastic forces inside a polymer, which are proportional to temperature (see e.g. ref 41), will contribute to the kinetics in a way that will not impart any temperature dependence to the (k_s/k_α) ratio. We will briefly discuss these entropic forces in this section.

The (k_s/k_α) ratio discussed in ref 1, though almost temperature independent, is noticeably smaller than one and varies from 10^{-1} to as low as 10^{-5} in the CO recombination experiment. We will see very shortly that this rate reduction is naturally related to the number of structurally distinct states the protein may visit before accomplishing a specific motion.

The rate of a diffusion-controlled relaxation process depends on the detailed geometry of the space explored by the diffusive process. It is possible to formulate a rather general, but somewhat abstract, argument to predict the rate that is largely independent of such geometry. Fortunately, in the case of low effective dimensionality of the relaxation, there is a familiar methodology we can use to test our understanding of relaxation with no (or low) intrinsic energetic barrier, namely the overdamped limit of Kramers theory. As is well-known, Kramers theory generalizes the transition state theory (TST) to include the effects of friction. By a barrier being low we mean it varies little on the length scales in the problem, including, *a fortiori*, the length of a typical diffusive step. More precisely, we stipulate that the transition state size must be larger than the particle mean free path: $l_{\text{mfp}} < l_{\text{TST}}$. In a high-temperature liquid the length l_{mfp} is literally a mean free path in the kinetic theory sense, but in the supercooled state it is the distance through which the protein relaxation reaction coordinate moves during a solvent reconfiguration event, i.e., the screened Lindemann length. The condition $l_{\text{mfp}} < l_{\text{TST}}$ formally corresponds to the overdamped limit of the TST expression for the reaction rate^{42,43}

$$k_{\text{damp}} = \frac{m\omega^*\omega_A}{2\pi\zeta} e^{-G^*/k_B T} \quad (9)$$

where ω_A is the frequency of the motion in the reactant well, ω^* is the barrier frequency, ζ is the friction coefficient, and G^* is the activation barrier. (G^* includes the transition state entropy and therefore is a free energy barrier.) Let us rewrite the expression in (9) in terms of relevant length and time scales. First of all $m\omega_A^2 l_A^2 \sim k_B T$, defines the “size” of the reactant region l_A , and $m\omega^{*2} l_{\text{TST}}^2 \sim k_B T$ defines the size of the transition state l_{TST} .⁴² Using the Stokes–Einstein relation $D = k_B T / \zeta$ and the usual $D = (1/2) l_{\text{mfp}}^2 k_{\text{mfp}}$, where k_{mfp}^{-1} is the mean collision time, one has up to an insignificant numerical factor:

$$k_{\text{damp}} = \frac{l_{\text{mfp}}^2}{l_A l_{\text{TST}}} k_{\text{mfp}} e^{-G^*/k_B T} \quad (10)$$

Once again, l_{mfp} and τ_{mfp} are the length and the time of each random step in the diffusive motion of the reaction coordinate. In the case of a solvent *above* T_A , those random steps are of the magnitude of the true kinetic theory mean free path. As argued earlier, in the case of slaving *below* T_A , the length and time are dictated by the surrounding stiff solvent that rearranges on time scale $1/k_\alpha$ from eq 2, producing molecular displacements of length d_L^{scr} inside the protein. Thus, $k_{\text{mfp}} = k_\alpha$ and $l_{\text{mfp}} = d_L^{\text{scr}}$. We leave the issue of the nonzero width of the k_α distribution for later. In the limit of zero barrier, i.e., $G^* = 0$, the reduction in the rate of an internal process relative to the solvent's relaxation rate reads

$$k_s/k_\alpha = \frac{(d_L^{\text{scr}})^2}{l_A l_{\text{TST}}} \quad (11)$$

In this limit, the size of the reactant region l_A and the transition state width l_{TST} become equal to the size of the whole “reactant” space, call it L , which is covered by the diffusive process. Alternatively, L is the physical length corresponding to the configurational space involved in this specific relaxation. One immediate consequence of this realization is that the rate reduction $k_s/k_\alpha = (d_L^{\text{scr}}/L)^2$ is more significant for processes which explore a larger configurational space. We will see shortly that if the effective dimensionality Δ of the diffusion is three

or higher, this reduction is inversely proportional to the “reactant” volume L^Δ , thus making the slaving experiments a convenient tool in determining how many structural states the protein explores in the course of a given reaction.

In a more abstract vein now, consider a particular relaxation process, subject to *no* intrinsic barrier, but which is a diffusion process in Δ effective dimensions. The control parameter of whether the reaction has occurred is the characteristic length L to travel from any initial location in the configurational space of the relaxation process to the “target” (of size d_T). Clearly, L is roughly the geometrical size of the region available to the diffusive process. (Even though Δ and L are so far defined in a rather detached manner, they will enter in the final answer in an easy to interpret and largely geometry independent combination.) The resulting rate is that of a diffusion controlled reaction as worked out (in 3D) by Smoluchowski. In general (for $\Delta \geq 3$), the corresponding rate coefficient will scale as $d_T^{\Delta-2}$ times the diffusion coefficient D . The total rate is obtained by multiplying the rate coefficient by the concentration $\sim L^{-\Delta}$ (we have a single diffusing “particle” only). The diffusion coefficient itself is, of course, directly related to the length l_{diff} of a typical step during the random walk and the time k_{diff}^{-1} it takes to make that step: $D = l_{\text{diff}}^2 k_{\text{diff}} / 2\Delta$ in Δ dimensions. In the slaved case, both scales are imposed by the solvent, namely $d_{\text{diff}} = d_L^{\text{scr}}$ and $k_{\text{diff}} = k_\alpha$. The resultant inverse of the time it takes to reach the target (up to a numerical constant) is $k_s \sim k_\alpha (d_L^{\text{scr}})^2 d_T^{\Delta-2} / L^\Delta$ yielding for the corresponding rate reduction:

$$k_s/k_\alpha \sim \frac{(d_L^{\text{scr}})^2 d_T^{\Delta-2}}{L^\Delta} \quad (12)$$

This relation shows how the relaxation rate is reduced due to the large size of the configurational space corresponding, for example, to the alternative locations of the ligand inside the protein and the different protein conformations. Indeed, the lower bound for the just estimated value of k_s/k_α is $(d_L^{\text{scr}}/L)^\Delta$, because d_L^{scr} is the smallest structurally discernible displacement in the system. For the same reason, $(L/d_L^{\text{scr}})^\Delta \equiv N_{\text{st}}$ provides a count of states available in the diffusion process in terms of structurally distinct states of the protein as imposed by the solvent motional constraints. The relation of N_{st} to the multiplicity of substates within a given subset of conformational states of the protein will be discussed later in the paper. It is in the combination L^Δ that the parameters L and Δ acquire a clear physical meaning, namely the *volume* of the conformational space of the relaxation process in question. Furthermore, since $k_s/k_\alpha \geq N_{\text{st}}^{-1}$, we arrive at the simple result that the inverse of the rate reduction k_s/k_α gives a lower bound on the number of distinct structural substates in the conformational space explored during the relaxation. A more detailed version of the argument above, but in a specific—spherical—geometry, is given in Appendix A. It not only yields the same qualitative conclusions but also provides specific values of numerical factors that vary depending on the geometry. Finally, note that the inverse of the rate reduction k_s/k_α is equal to the ratio of the total relaxation time to that of single solvent induced rearrangement. Thus this inverse ratio may be thought of, informally, as the number of elemental steps that are typically necessary to accomplish the (slaved) relaxation.

Next, we discuss how the size of the cooperatively rearranging region ξ of the liquid relative to the protein’s dimensions influences the statistics of slaving time scales and how the distribution of the latter is affected by the distribution $P(k_\alpha)$ of the liquid relaxation rates. Let us first analyze the most

straightforward case when the relaxation involves moving a solvent exposed segment of the protein that is smaller than ξ in size, such as hinge-like motion of a short arm of the protein, perhaps a local helix unfolding. In this case, each step of the segment’s walk will exactly follow the kinetics of the nearby solvent. Such a situation represents a case of extreme slaving in that each diffusion step in the relaxation will be of the bare length d_L . To complete the relaxation, many small consecutive structural changes must occur. In our earlier language, these changes correspond to diffusion steps whose time span is actually distributed because the solvent’s relaxation time distribution $P(k_\alpha)$ has a nonzero width. Therefore we must determine how eqs 11 and 12 are affected by the distribution. When introducing a rate distribution $P(k_\alpha)$, one adopts the view that each elemental relaxation is nearly exponential and that the nonexponentiality observed in bulk is due to space and time inhomogeneity in the local environment. Viewed this way, the local relaxation rate k_α is a *quenched* variable that does not change on the time scale of a local process, or whose change in time is decoupled from the relaxation itself. Extensive variables can be averaged over the quenched disorder. Examples are free energy and its derivatives with respect to intensive variables, such as response functions. Therefore, a proper way to extract the relaxation rates of a slaved process is, for example, to analyze its response function as averaged over $P(k_\alpha)$. Indeed, the usually reported relaxation rate of a supercooled liquid, k_α , is the frequency at the maximum of the imaginary part of the response in frequency domain

$$\left\langle \frac{\omega k_\alpha}{k_\alpha^2 + \omega^2} \right\rangle_{k_\alpha} \quad (13)$$

where the angular brackets denote averaging wrt $P(k_\alpha)$. The solvent’s relaxation rate k_α , used in the earlier arguments as determining the generic time scale of a diffusion step, is a distributed variable. The response function above must be averaged according to the distribution. Such averaging already takes place, to a degree, if the diffusion involves many steps. Now, the *total* relaxation time $1/k_s$ of the slaved process is, roughly speaking (see Appendix B), a *sum* of elemental times taken from the distribution $P(k_\alpha)$. Therefore, inasmuch as the most probable value of the $P(k_\alpha)$ distribution is related to its mean, the most likely value of k_s , as the one maximizing the response function of the slaved process, is indeed simply the most likely value of k_α rescaled by the reduction factor from eq 11 or eq 12. What about the *width* of the $P(k_s)$ distribution? Qualitatively, it is clear that the width will be smaller, in proportion to the distribution mean, for a larger number of steps (roughly $N_{\text{step}}^{-1/2}$ for a Poissonian diffusive process) and hence for a larger number of states N_{st} . The first corollary of this is that the mean and the most probable values of the $P(k_s)$ distribution do indeed become closer for slower processes, consistent with our earlier notion that a k_α distribution does not introduce a temperature dependence into the k_s/k_α ratio. Perhaps more interesting consequences become apparent upon noting that the width of a relaxation time distribution is directly related to the (non-)exponentiality of the corresponding process, with broader distributions corresponding to more nonexponential processes (see e.g. ref 5). This implies that processes with greater rate reduction, that span larger conformational subspaces, will also be more exponential! While we illustrate some of the ideas above in Appendix B, it may suffice to note that this narrowing of the relaxation rate distribution is an (disguised) example of motional narrowing (see also ref 44).

The precise amount of nonexponentiality will depend not only on the $P(k_\alpha)$ distribution but also on the distribution of the number of steps N_{step} necessary to accomplish the relaxation: the gross rate reduction k_s/k_α reflects only the *nominal* number of steps. Furthermore, presenting the conformational space of the protein as a featureless multidimensional manifold is naive; one can imagine there exist relaxations—especially if the corresponding N_{st} is large—that have a few short-cuts, which, while entropically costly, require a small number of steps. This would *also* lead a narrowing down of the rate distribution and thus an enhanced exponentiality. Note that the latter scenario corresponds, in a sense, to an entropy crisis in the space of relaxation routes—and hence the “space” of rate coefficients, as discussed by Wang, Onuchic, and Wolynes.⁴⁵

Finally, the correlation between the rate reduction and the degree of nonexponentiality is consistent with earlier findings of ref 13. One must bear in mind, however, that owing to the overall rescaling of the relaxation curve toward slower times, a shorter portion of the curve (corresponding to less decay) will be available from experiment, and so the degree of nonexponentiality will be harder to assess quantitatively. Furthermore, when comparing two decay profiles, corresponding to different degrees of the rate reduction, k_s/k_α , only the data above the smallest detected population of the *slower process* can be used.

It seems instructive to note a distinction between the case of solvent exposed segment's motion and the purely hydrodynamic effects of the k_α distribution, such as translation diffusion of a Brownian particle, derived in ref 6. In the former situation the total relaxation rate is diminished (compared to the solvent) due to the many steps needed to complete the process, while in the latter case there is an apparent enhancement of the translational diffusion coefficient for particles smaller than ξ ! The difference is understood by recalling that in the slaved case the diffusion coefficient $\propto d_L^2 k_\alpha$ does not characterize *self*-diffusion but rather reflects the length and time scales of structural reconfiguration in the liquid at the molecular level. The structural rearrangements result in the reaction coordinate progressing on those time and length scales. In contrast, the “macroscopic” diffusion coefficient describes the low-frequency response to an *external* force and is essentially the average of the inverse viscosity ($\propto \langle k_\alpha \rangle$), which will obviously favor the larger k_α 's thus enhancing the self-diffusion coefficient. ($\langle k_\alpha \rangle$ naturally arises in hydrodynamics because it is proportional to the average molecular autocorrelation time $t_{\text{auto}} = 1/m\zeta$.) At the same time, the *length* scale of a translation is arbitrary and determined by the externally (or thermally), but not structurally, imposed velocity amplitude.

In contrast to the just discussed case of motions that are directly solvent exposed, the influence of the solvent on most *internal* processes is more indirect. It comes from the many domains surrounding the protein and is propagated inside the molecule via the protein's elasticity, because the size of the whole protein is normally larger than ξ . One possibility is that not every external structural change in the solvent causes a translation of the internal reaction coordinate, as if the latter skipped some of the (irregular) beats imposed by the solvent. Such a situation, analyzed in the following subsection, is only important if it implies the existence of an unavoidable steep internal energy barrier. We now consider the two extreme *a priori* cases of purely elastic and of purely glassy folded protein lattices which should cover the whole range of entropic barriers. Both limiting cases yield similar conclusions. The obvious difference with the exposed segment situation, discussed earlier, is that there are more domains which may influence an internal

process. However the domains are now further away, and their effect is thus screened by the protein's bulk (see Figure 3 and its caption). In the elastic case, for a protein not much bigger than ξ , the screened Lindemann length for a relaxation occurring right in the middle of the protein is generically $d_L^{\text{scr}} \sim d_L/2$. The number of surrounding domains would vary depending on the biomolecule's size and the temperature, but is of order 10^1 . Therefore the k_{diff} would be amplified by the same factor. The resultant diffusion coefficient $\propto (d_L^{\text{scr}})^2 k_{\text{diff}}$ is still similar to the exposed case. Note, for the sake of argument, that if the protein's size d_{pr} were *very* large, so that $d_{\text{pr}} \gg \xi$ and $d_L^{\text{scr}} \sim d_L(\xi/d_{\text{pr}})^3$, one would obtain a much smaller diffusion coefficient that scales as $(d_L^2 k_\alpha)(\xi/d_{\text{pr}})$.⁴ Notwithstanding the possibility of a purely elastic scenario, experiment shows that the energy landscape of a *folded* protein still has a large number of minima.^{17,46,47} This fact implies that structurally and dynamically, the molecule near its native state is barely different from its supercooled solvent! The glassy case is therefore even simpler, and the earlier analysis of the extreme slaving situation applies automatically here.

Last, we raise the issue of the relaxation being possibly coupled to entropic forces inside the protein, such as the ones giving rise to rubber elasticity, and which are proportional to the temperature. This entropic force is all that exists in an extended chain according to Kuhn's theorem. On the other hand, within a collapsed polymer, there are also excluded volume and attractive van der Waals forces as well as the elasticity of the molecular bonds. These give rise to the so-called “intrinsic viscosity” of polymers.⁴⁸ If they are important, a definitive conclusion on this issue would require a detailed analysis in each specific case. In all likelihood, temperature independent pure elastic forces from those sources will make some contribution in determining the equilibrium relative positions of the molecular subunits of the protein. In this case, the total local elastic coefficient will have a temperature independent component and thus give rise to a T -independent portion of the corresponding barrier and to an additional Arrhenius-like temperature dependence of k_s/k_α .

As a result, the following picture of slaving in the case of no intrinsic barrier emerges. Depending on how many intrinsic states there are to a slaved process, one obtains a range of possible kinetic scenarios. In the case of a small conformational space, complete slaving occurs, with the relaxation faithfully following that of the solvent, including the details of nonexponentiality. Automatically, $k_s/k_\alpha \sim 1$ here. In the opposite limit of many diffusive steps (corresponding to $N_{\text{st}} \gg 1$), one still gets $k_s/k_\alpha \sim \text{const}$, where the constant is now smaller than one and scales with N_{st}^{-1} . Here, surprisingly, the internal process would be closer to exponential than the solvent's kinetics. A detailed analysis of the nonexponentiality of the solvent and the protein relaxation will give more insight into slaving.

4.2. Case 2: Internal Barrier. The results of the previous subsection can be easily applied to a more complicated case when there *is* an internal barrier intrinsic to the protein even in the absence of slaving. Let us assume for now that the height of this internal barrier is independent of the solvent's configuration. Otherwise, one has a case of gating, on which we will comment briefly later. We have already considered the case of a broad barrier, where $l_{\text{TST}} \gg d_L^{\text{scr}}$. In this situation, one may use the Kramers formula in the overdamped regime, as in eq 10, now with $G^* > 0$. It may be instructive to express the solvent's relaxation rate k_α through the corresponding relaxation barrier according to eq 2. One immediately observes that the total barrier is the sum of the internal one and the one for the

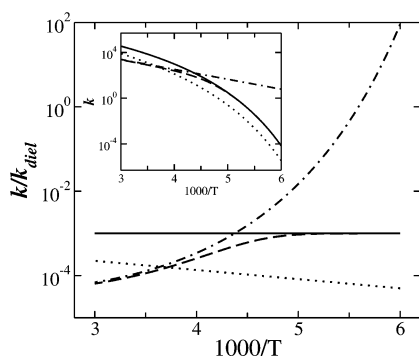


Figure 4. The behavior of k_s/k_α as a function of inverse temperature for various parameter values. The T -dependence of the solvent's dielectric relaxation rate (not shown on the graph) is assumed to obey a Vogel–Fulcher law according to $k_\alpha \propto \exp\{1200K/T - 120K\}$. The solid line illustrates a simple barrierless behavior, when no internal energetic barrier is present, with rate reduction 10^{-3} . The dashed curve shows the slaved process with a narrow (sufficiently high) intrinsic barrier. The dashed–dotted line is the same, but if no slaving is present. The dotted line is the simple barrierless case, depicted by the solid line, but with an additional broad barrier of height ~ 4 kJ/mol, as emulated here by an additional factor of $\exp(-500K/T)$. Clearly, the overall shift of the curve down from the barrierless case is comparable to the variation of the curve's ordinate within this temperature range. The inset shows the same rates as the main plot but not divided by the solvent's k_α .

liquid rearrangements. The prefactor $\propto d_L^2 k_{\text{micro}}^{-1}$ does not have a clear meaning anymore, because k_{micro}^{-1} is the mean-collision time *above* T_A , whereas d_L is a length scale relevant *below* T_A , but this is quantitatively unimportant. A nonzero $\partial(G^*/T)/\partial(1/T)$ exhibits itself by a slope in the $1/T$ dependence of k_s/k_α . An example of such a dependence is shown by the dotted line in Figure 4. Here, we took the barrier to be about 4 kJ/mol (more precisely, it is $3k_B T_0$, where T_0 is the lower end of the T range on the graph). Graphing a slaved process with such an additional barrier is instructive in more than one way. First of all, a barrier that is large enough to give a discernible slope also implies an overall “uniform” reduction in rate (see the Figure 4 caption). Therefore, if such a slope exists but is disregarded, the purely entropic contribution to the rate reduction might be significantly overestimated.

A distinct physical situation arises when the barrier is narrow, so that $l_{\text{TST}} < d_L^{\text{scr}}$. Here, overcoming the internal barrier and the reaction coordinate displacement due to the solvent's rearrangements are *sequential* processes, if the barrier is steep enough. The total rate will then be determined by the speed of the rate limiting step. The steepness of the barrier comes about in the following way. If the internal barrier is sufficiently low, one can expect that a solvent rearrangement will “carry” the system over the barrier, as if the barrier did not exist (remember, $l_{\text{TST}} < d_L^{\text{scr}}$). On the other hand, if the relaxation cannot proceed further unless it overcomes the bottleneck of a steep barrier, the elastic force due to a regular distortion of the protein by the stiff solvent may not be sufficient to change the reaction configuration. Indeed, the amount of elastic energy stored by the protein in a molecular volume a ,³ when a distortion d_L^{scr}/a is present, is approximately $\mu a (d_L^{\text{scr}})^2$, where μ is the elastic coefficient. On the other hand, the work needed to move the reaction coordinate up the barrier by distance δl is about $|\partial V/\partial x| \delta l$. Equating the two energies gives an estimate of the maximum displacement of the reaction coordinate due to the solvent's rearrangements. If it turns out that $\delta l < l_{\text{TST}}$, then the rate-limiting step is the internal barrier crossing. The temperature dependence of k_s/k_α in this situation is exemplified by the dashed

line in Figure 4, assuming the height of the internal barrier is independent, within d_L , of the protein's shape changes. Here, the ratio of the relaxation rates grows with decreasing temperature as the Vogel–Fulcher barrier rapidly approaches the internal barrier in value, and the k_s/k_α levels off below a certain value of T . On the other hand, if the internal barrier height is strongly dependent on the solvent (this would constitute a case of solvent imposed gating), we are effectively back to the case of extreme slaving discussed in the previous subsection, although a behavior of the type as depicted by the “sequential process” (dashed) curve in Figure 4 may still be observed if there is a solvent independent (and significant) component to the internal barrier.

4.3. Determining the Entropy of Conformational Substates using Slaving Experiments. Averaging Issues and Single Molecule Spectroscopy. We devote this brief subsection to the question whether one can use information obtained in slaving experiments to deduce the multiplicity of conformational substates or the entropy of a protein in its native state. Since this entropy is vastly smaller than that of the unfolded state, it is often assumed to be zero for the lack of a better estimate. There are situations, however, where a more precise value of the native state entropy is desirable. An example would be a protein that could be only partially folded and would still be biologically active.⁴⁹ A more extreme case would be a situation where the protein only will fold when in contact with its target, as in the fly casting mechanism.⁵⁰

Each slaved process explores only a fraction of the conformational substates in the native state. Regardless of how significant the fraction is, it definitely provides a *lower* bound for the native state's entropy. We therefore suggest that the biggest rate reduction found in a process with no intrinsic barrier provides us with such a lower bound. If two distinct processes can be shown to be independent, then their respective contributions should be simply summed together, and so forth for a larger number of independent relaxation modes. The question is now how the quantity N_{st} is related to the number of substates in the native basin at biologically relevant conditions. N_{st} is the substate count as expressed in terms of distinct structural substates as imposed by the solvent. Such number, as computed or measured in the supercooled solvent itself, would be *the* measure of the configurational freedom for the following reason. Since the Lindemann length d_L is the smallest structurally discernible translation of a molecular unit from the point of view of solvent dynamics, the total number of substates explored by a collection of N molecules is, roughly, $(l/d_L)^{3N}$, where l is the generic size of a region a molecule could explore during thermal equilibration. On the other hand, more conventional attempts to enumerate distinct substates within the native basin have to do with counting the alternative rotamer states or relative positions of the secondary structure units, etc. However, that is not the only way to accomplish such an enumeration. The Lindemann length of the side chain is often the relevant length scale in the polymer treatments of heteropolymer glass transition and folding. Indeed, it has been shown that even though at the gross level the protein folding landscape always has a kinetically sensed slope toward the native basin, near that basin, the free energy surface of the molecule is a caldera that has many substates, perhaps as many as a plastic crystal. The total number of substates in this basin is the conformational entropy of the folded protein, and it is legitimate to count those substates the same way they are counted in the liquid, except now the regular Lindemann length is replaced by the screened one, d_L^{scr} . We remind the reader that d_L^{scr} is the bigger of the two displace-

ments: one is caused by elastic propagation of the external molecules' relative displacements inside the protein, the other signifies distinct relative positions of the internal molecular units. Thus the biggest reduction of an internal rate that can be imagined depends on the native state entropy.

In any macroscopic sample, different protein molecules reside in nonequivalent internal substates. This inhomogeneity is partly driven by the inhomogeneity of the external environment, provided by the mosaic structure of supercooled liquids and the hydration shell. This notion supports the importance of performing single molecule studies of slaving, as the variation of a local signal may provide a lot more detail than the averaged out response, for example it may give a much more realistic estimate of the native state entropy.

Acknowledgment. The authors thank Garegin Papoian and Johan Ulander for useful conversations. H.F. acknowledges the support from the Department of Energy Contract W-7405-Eng-36 and the Laboratory Directed Research and Development program of the Los Alamos National Laboratory. He also thanks Ben McMahon, Paul Fenimore, and Bob Young for illuminating discussions. The work of P.G.W. was supported by NIH grant 5R01GM44557 and NSF Che 0317017.

Appendix A. Smoluchowski Rate in Δ Dimensions

Here, we supplement the dimensional argument leading to eq 12 by analyzing the simplest case: the spherically symmetrical geometry. At the same time, this will give the reader a feel of what the omitted numerical constants may be. The stationary solution of the diffusion equation (obeying $\nabla^2 n = 0$, n concentration) that is equal to unit concentration far from the target: $n = 1$ ($r \rightarrow \infty$) and zero at the target: $n = 0$ ($r = R_T$) is $n(r) = 1 - (R_T/r)^{\Delta-2}$ (for $\Delta \geq 3$). The resulting rate coefficient—the flux into the target (at unit concentration)—is $S_{\Delta} R_T^{\Delta-1} D |(\partial n / \partial r)_{r=R_T}|$, where $S_{\Delta} = 2\pi^{\Delta/2} \Gamma(\Delta/2)$ is the area of a unit sphere in Δ dimensions. The total rate is obtained by multiplying this expression by the “particle concentration” (i.e. one per total volume) $1/(S_{\Delta} L^{\Delta})$ to yield (for $L \gg R_T$):

$$\frac{k}{k_{\alpha}} = \frac{\Delta - 2}{2} \frac{(d_L^{\text{scr}})^2 R_T^{\Delta-2}}{L^{\Delta}} \quad (\Delta \geq 3) \quad (\text{A.1})$$

where we have used $D = (d_L^{\text{scr}})^2 k_{\alpha} / 2\Delta$, as before, and R_T and d_T are equal within a factor of order unity: $d_T = R_T (S_{\Delta} / \Delta)^{1/\Delta}$. We stress though that no special significance should be given to the numerical factor in the front as it will vary for different geometries (nevertheless the factor $(\Delta - 2)$ will persist). Finally, we note that cases $\Delta = 2$ and $\Delta = 1$ are somewhat underdefined, in view of the multiplicity of the degrees of freedom involved in each process. However we do provide the corresponding answer for the reader's reference. Those are respectively $(d_L^{\text{scr}} / L)^2 / 2 \ln(L/R_T)$, $\Delta = 2$ and $(d_L^{\text{scr}} / L)^2$, $\Delta = 1$, consistent with an earlier result obtained from the Kramers theory.

What are the Δ values one may reasonably expect for a typical relaxation involving structural rearrangement of the protein? Let us consider, for the sake of the argument, a process in which a ligand travels a distance comparable to its own size but leaves the protein unchanged. Call the molecular scale in a protein a_{pr} , in distinction with the solvent's a . a_{pr} is bound from below by the thickness of a residue, say 3 Å. This yields $d_L^{\text{scr}} \sim 0.3$ Å. The “target” size is probably limited by the size of the ligand itself, say 2 Å. $\Delta = 3$ would give, according to eq 1, a rate reduction of size 0.01. A smaller target size will make the rate reduction significantly more sensitive to the effective dimen-

sionality. So, for example, for $R_T = L/2$ and $\Delta = 6$, the rate reduction would be about $3 \cdot 10^{-3}$. $\Delta = 6$ may imply, for instance, two particles diffusing independently, each in 3D. This corresponds to an effective two-particle (plus bath) process, say the ligand plus one residue, or two residues with three constraints, etc. $\Delta = 9$ yields $k_s/k_{\alpha} \approx 6 \cdot 10^{-4}$, $\Delta = 15$ results in $k_s/k_{\alpha} \approx 2 \cdot 10^{-5}$ and so forth.

Appendix B: Narrowing of the Relaxation Rate Distribution

In distinction with the main text, in this Appendix we use the relaxation *times* of the solvent, not rates: $\tau \equiv 1/k_{\alpha}$.

First note that a slower-than-exponential process can always be presented (at long enough times) as a superposition of exponential processes, so that the corresponding waiting time distribution (WTD) is $\psi(t) = \int (d\tau/\tau) e^{-t/\tau} P(\tau)$, where $P(\tau)$ is a distribution of relaxation times (not to be confused with waiting times). If $P(\tau)$ is slower than exponential, it is easy to convince oneself—that $\psi(t) = P(t)$ for long enough times t (see e.g. ref 51), and so one can use interchangeably the concepts of *waiting* and *relaxation* times for such processes, and at long times.

Next, what is the waiting time distribution $\psi_N(t)$ of a process consisting of N steps such that the WTD of an individual step is $\psi(t)$? In a standard way

$$\psi_N(t) = \sum_{i=1}^N t_i = \int_{-\infty}^{\infty} \frac{d\lambda}{2\pi} e^{i\lambda t} \left[\int d\tau \psi(\tau) e^{-i\lambda \tau} \right]^N \quad (\text{B.1})$$

For example, for Poisson processes, $\psi(t) = \gamma e^{-\gamma t}$, it is easy to show that $\psi_N(t) = \gamma(\gamma t)^{N-1} / (N-1)! e^{-\gamma t}$. Clearly, the transition probability of the process $\psi_N(t)$ is well localized at $t = N/\gamma$, that is at the N -multiple of the characteristic, *relaxation* time $1/\gamma$. Therefore, at times $t \sim N/\gamma$, one may think of the $\psi_N(t)$ process as an exponential process with relaxation rate γ/N . (In contrast, at short times the survival probability $p_N(t) = 1 - \int_0^t d\tau \psi_N(\tau) \sim 1 - (\gamma t)^N / N!$ decreases significantly slower than as prescribed by $e^{-\gamma t/N}$.) Similar conclusions, although not as easily seen explicitly, apply to other WTD's with a finite mean $1/\gamma$ as well.

The two notions above show that the *relaxation* time of an N -step process, whose individual step WTD's are identical and slower than exponential, is itself distributed as the sum of the individual *relaxation* times.

Now, let us write out the simplified log-normal relaxation time, τ , distribution, alluded to in the discussion of eq 7

$$P(\ln \tau) = \frac{1}{\sqrt{2\pi}(\delta F^{\ddagger}/T)} e^{-\ln^2(\tau/\tau_{\text{mp}})/2(\delta F^{\ddagger}/T)^2} \quad (\text{B.2})$$

where τ_{mp} is the most probable relaxation time corresponding to the most probable barrier: $\tau_{\text{mp}} = \tau_{\text{micro}} e^{F_{\text{mp}}^{\ddagger}/T}$. The barrier distribution is assumed to be a Gaussian centered around F_{mp}^{\ddagger} , with a width δF^{\ddagger} . The most nonexponential portion of the relaxation profile corresponding to $P(\tau)$ is observed at times such that $\ln(\tau/\tau_{\text{mp}})$ is small and can be well approximated by a stretched exponential (see e.g. ref 51), which is indeed frequently used to fit various relaxation profiles in supercooled liquids. (Note, owing to the large magnitude of τ_{mp} , even the relatively small values of $\ln(\tau/\tau_{\text{mp}})$ correspond to a sizable time interval.) It will suffice for our purposes here to consider times τ close enough to τ_{mp} so that one can Taylor expand the logarithm in eq 2. At such times, the τ distribution is Gaussian with $\delta\tau/\tau_{\text{mp}} = \delta F^{\ddagger}/T$ (cf. eq 7). Clearly, the effective relaxation rate of a sequence of N such processes will be distributed, at times close

enough to $N\tau_{\text{mp}}$, according to a Gaussian with the relative width $\delta\tau_N/(N\tau_{\text{mp}}) = N^{-1/2}(\delta F^*/T)$. In the time frame rescaled by the number of steps N , the distribution is indeed more narrow, resulting in less nonexponentiality.

A few final remarks. At times longer than $N\tau_{\text{mp}}$ the process will appear more and more exponential, because the real $P(\tau)$ is practically cut off at τ_{mp} (see the main text). At times much shorter than $N\tau_{\text{mp}}$, when the Taylor expansion becomes inaccurate, the conclusions above still apply qualitatively. Perhaps more importantly, at these shorter times, more detailed knowledge of the N distribution (and hence the relaxation morphology) is necessary for quantitative analysis. Additionally, "short-cut" processes, mentioned in the main text, may take place.

References and Notes

- (1) Fenimore, P. W.; Frauenfelder, H.; McMahon, B. H.; Parak, F. G. *Proc. Natl. Acad. Sci.* **2002**, *99*, 16047.
- (2) Ringe, D.; Petsko, G. A. *Biophys. Chem.* **2003**, *105*, 667.
- (3) Kirkpatrick, T. R.; Thirumalai, D.; Wolynes, P. G. *Phys. Rev. A* **1989**, *40*, 1045.
- (4) Xia, X.; Wolynes, P. G. *Proc. Natl. Acad. Sci.* **2000**, *97*, 2990.
- (5) Xia, X.; Wolynes, P. G. *Phys. Rev. Lett.* **2001**, *86*, 5526.
- (6) Xia, X.; Wolynes, P. G. *J. Phys. Chem. B* **2001**, *105*, 6570.
- (7) Lindemann, F. A. *Phys. Z.* **1910**, *11*, 609.
- (8) In ref 1, we denoted these fluctuations by k_{diel} . To be consistent with recent results, given in ref 9, we switch to notation $k_a(T)$ that stresses similarities with fluctuations in glasses.
- (9) Fenimore, P. W.; Frauenfelder, H.; McMahon, B. H.; Young, R. D. *Proc. Natl. Acad. Sci.* In press.
- (10) Austin, R. H.; Beeson, K. W.; Eisenstein, L.; Frauenfelder, H.; Gunsalus, I. C. *Biochemistry* **1975**, *14*, 5355.
- (11) Kleinert, T.; Doster, W.; Leyser, H.; Petry, W.; Schwarz, V.; Settles, M. *Biochemistry* **1998**, *37*, 717.
- (12) Johnson, J. B.; Lamb, D. C.; Frauenfelder, H.; Muller, J. D.; McMahon, B.; Nienhaus, G. U.; Young, R. D. *Biophys. J.* **1996**, *71*, 1563.
- (13) Frauenfelder, H. et al., *J. Phys. Chem.* **1990**, *94*, 1024.
- (14) Scholl, R. W. Ph.D. Thesis, University of Illinois at Urbana-Champaign, 1994.
- (15) Shibata, Y.; Kurita, A.; Kushida, T. *Biochemistry* **1999**, *38*, 1789.
- (16) Huck, J. R.; Noyel, G. A.; Jorat, L. J. *IEEE Trans. Electron. Ins.* **1988**, *23*, 627.
- (17) Frauenfelder, H.; Sligar, S. G.; Wolynes, P. G. *Science* **1991**, *254*, 1598.
- (18) Yang, F.; Phillips, G. N. *J. Mol. Biol.* **1996**, *256*, 762.
- (19) Lubchenko, V.; Wolynes, P. G. *J. Chem. Phys.* **2004**, *121*, 5958.
- (20) Kauzmann, W. *Chem. Rev.* **1948**, *43*, 219.
- (21) Richert, R.; Angell, C. A. *J. Chem. Phys.* **1998**, *108*, 9016.
- (22) Mezei, F. In *Liquids, Freezing and the Glass Transition*; Hansma, J. P., Levesque, D., Zinn-Justin, J., Eds.; North-Holland, Amsterdam, 1991; p 629.
- (23) Singh, Y.; Stoessel, J. P.; Wolynes, P. G. *Phys. Rev. Lett.* **1985**, *54*, 1059.
- (24) Stoessel, J. P.; Wolynes, P. G. *J. Chem. Phys.* **1984**, *80*, 4502.
- (25) Wolynes, P. G. *Acc. Chem. Res.* **1992**, *25*, 513.
- (26) Kirkpatrick, T. R.; Thirumalai, D. *Transp. Theor. Stat. Phys.* **1995**, *24*, 927 and references therein.
- (27) Villain, J. *J. Physique* **1985**, *46*, 1843.
- (28) Ostwald, W. Z. *Phys. Chem.* **1897**, *22*, 289.
- (29) Stranski, I. N.; Totomanow, D. Z. *Phys. Chem.* **1933**, *163*, 399.
- (30) Lubchenko, V.; Wolynes, P. G. *Phys. Rev. Lett.* **2001**, *87*, 195901.
- (31) Wolynes, P. G. In *Proceedings of the International Symposium on Frontiers in Science (Hans Frauenfelder Festschrift)*, Chan, S., DeBrunner, P. G., Eds. (Am. Inst. Physics, 1989).
- (32) Ehrenfest, P.; Ehrenfest, T. *The Conceptual Foundations of the Statistical Approach in Mechanics*; Dover, 1990.
- (33) Lubchenko, V.; Wolynes, P. G. *J. Chem. Phys.* **2003**, *119*, 9088.
- (34) Leutheusser, E. *Phys. Rev. A* **1984**, *29*, 2765.
- (35) Kirkpatrick, T. R.; Wolynes, P. G. *Phys. Rev. A* **1987**, *35*, 3072.
- (36) Tracht, U.; Wilhelm, M.; Heuer, A.; Feng, H.; Schmidt-Rohr, K.; Spiess, H. W. *Phys. Rev. Lett.* **1998**, *81*, 2727.
- (37) Lubchenko, V.; Wolynes, P. G. *Proc. Natl. Acad. Sci. U.S.A.* **2003**, *100*, 1515.
- (38) Swallen, S. F.; Bonvallet, P. A.; McMahon, R. J.; Ediger, M. D. *Phys. Rev. Lett.* **2003**, *90*, 015901.
- (39) de Gennes, P. G. *Scaling Concepts in Polymer Physics*; Cornell University Press: 1979.
- (40) Onuchic, J. N. private communication.
- (41) Grosberg, Yu.; Khokhlov, A. R. *Statistical Physics of Macromolecules*; AIP Press: 1994.
- (42) Frauenfelder, H.; Wolynes, P. G. *Science* **1985**, *229*, 337.
- (43) Hänggi, P.; Talkner, P.; Borkovec, M. *Rev. Mod. Phys.* **1990**, *62*, 251.
- (44) Lubchenko, V.; Silbey, R. J. *J. Chem. Phys.* **2004**, *112*, 5958.
- (45) Wang, J.; Onuchic, J. N.; Wolynes, P. G. *Phys. Rev. Lett.* **1996**, *76*, 4861.
- (46) Frauenfelder, H.; Petsko, G. A.; Tsernoglou, D. *Nature* **1979**, *280*, 558.
- (47) Ansari, A.; Berendzen, J.; Bowne, S. F.; Frauenfelder, H.; Iben, I. E. T.; Sauke, T. B.; Shyamsunder, E.; Young, R. D. *Proc. Natl. Acad. Sci.* **1985**, *82*, 5000.
- (48) Doi, M.; Edwards, S. F. *The Theory of Polymer Dynamics*; Clarendon Press: 1988.
- (49) Vamvaca, K.; Vögeli, B.; Kast, P.; Pervushin, K.; Hilvert, D. *Proc. Natl. Acad. Sci.* **2004**, *101*, 1286.
- (50) Shoemaker, B. A.; Portman, J. J.; Wolynes, P. G. *Proc. Natl. Acad. Sci.* **2000**, *97*, 8868.
- (51) Castaing, B.; Souletie, J. *J. Phys. I* **1991**, *1*, 403.